This article has been accepted for publication in a future proceedings of this conference, but has not been fully edited. Content may change prior to final publication.
Citation information: DOI: 10.1109/UPEC65436.2025.11279803, 2025 60th International Universities Power Engineering Conference (UPEC)

A Comprehensive Design and Simulation of Highly Inductive Bi-directional Wireless Power Transfer.

Chethan Talkad Keshavamurthy
FEV UK Ltd.
Coventry, UK
keshavamurthy@fev.com

Payal Rajendra Chavan
Department of Electronic and Electrical Engineering
Brunel University of London,
London, UK
cm.payalrajendra@gmail.com

Mohamed Darwish
Department of Electronic and Electrical Engineering
Brunel University of London,
London, UK
mohamed.darwish@brunel.ac.uk

Abstract— This paper presents the design and optimization of a Bidirectional Wireless Power Transfer (BWPT) system for electric vehicles (EVs), enabling efficient two-way energy exchange between the grid and vehicle. The proposed system integrates with smart grids and renewable sources, enhancing sustainability. Robust control strategies manage smooth transitions between Grid-to-Vehicle (G2V) and Vehicle-to-Grid (V2G) modes to maintain stability. Key design aspects – including component selection with appropriate ratings, resonant tuning, and alignment – are optimized to maximize efficiency and minimize losses. The system is modeled and simulated in MATLAB/Simulink under realistic conditions, demonstrating high performance: efficiency reaches 97.4% in G2V mode and 90.25% in V2G mode. These results highlight the practical viability of the BWPT design for future EV charging infrastructure.

Keywords— *BWPT – Bidirectional wireless power transfer, IPT – Inductive power transfer, Vehicle-to-Grid (V2G), Grid-to-Vehicle (G2V), Resonant Compensation (LCC).*

I. INTRODUCTION

Wireless Power Transfer (WPT) enables electrical energy transmission without physical interactions, offering safety, reliability, and convenience. Traditional unidirectional WPT systems support only Grid-to-Vehicle (G2V) energy flow. In contrast, Bidirectional Wireless Power Transfer (BWPT) systems facilitate both G2V and Vehicle-to-Grid (V2G) operations, and in some cases, Vehicle-to-Home (V2H), allowing EVs to operate as distributed energy resources. According to the International Energy Agency (IEA), global EV sales reached approximately 14 million in 2023, marking a 35% increase from 2022 [1]. This growth is driven by advancements in battery technologies, environmental awareness, and favorable government policies [2]. Fig. 1 presents a simplified schematic of a wireless EV charging system. This paper focuses on the design and development of an efficient BWPT system, addressing key challenges and optimizing performance for real-world applications. Inductive Power Transfer (IPT), a widely adopted WPT technology, employs loosely coupled magnetic fields to achieve efficiencies exceeding 90% [6]. A bidirectional IPT system can be constructed by adapting unidirectional IPT frameworks. To maintain focus and technical depth, several areas are excluded from the scope of this study:

- **Thermal Management**: Analysis of heat dissipation and cooling mechanisms is beyond the scope.
- **Renewable Energy Integration**: While important, modelling renewable variability is outside the current work.
- **Economic Modelling**: Detailed cost-benefit analysis and financial feasibility studies are not addressed.

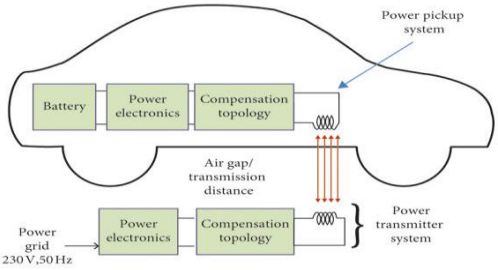

Figure 1: "Configuration of the EV wireless charging system" [11]

The overarching goal is to propose robust control strategies for bidirectional power flow, ensuring reliable performance under diverse operational conditions. BWPT systems, when integrated with energy storage and renewable resources, can reduce grid dependency in microgrids [12]. Stationary Energy Storage Systems (SESS) further enhance system reliability by compensating for the intermittent nature of renewable sources and ensuring backup during power disruptions [13].

II. LITREATURE REVIEW

Bidirectional Wireless Power Transfer (BWPT) systems integrated with grid-connected energy storage are gaining traction for enhancing Electric Vehicle (EV) charging and Vehicle-to-Grid (V2G) applications. Onar et al. [7] developed a 20 kW BWPT system using a double-sided LCC/LCC topology, operating at 22 kHz across an 11-inch air gap to accommodate high ground clearance. The system supports asymmetric voltages (800 VDC/350 VDC) and achieves 92.7% grid-to-vehicle efficiency, serving as a foundational reference for this study. [7] To address high current demands and low coupling conditions, larger pad sizes and reduced air gaps are employed to maximize mutual inductance. A Double-D coil configuration, as demonstrated in [14], enhances magnetic coupling and achieves efficiencies of 96.1% (G2V) and 96.2% (V2G), adhering to SAE J2954 standards for air gap and mutual inductance. Various BWPT topologies have been explored, including LCL resonant circuits and series-series (SS) compensation, with power ratings ranging from 1.5 kW to 20 kW [4], [6], [8]. For example, an LCL-based system with reversible rectifiers and a 4 cm air gap showed efficient power transfer under dynamic loads [6]. Coil design parameters such as wire gauge and core type significantly affect efficiency and operating range [4]. DC bus integration and phase shift control facilitate bidirectional power flow [8].

Control strategies range from H-bridge inverters functioning as buck/boost converters [3] to dual microcontroller systems with PI controllers and VCOs for phase and frequency synchronization [15]. Efficiency improvements up to 95.2% have been achieved using zero-voltage switching (ZVS) and multi-active-bridge (MAB) converters with LCC compensation [17]. DAB converters integrated with LCC

networks utilize fundamental harmonic analysis (FHA) to optimize resonant parameters within SAE J2954 frequency standards (65–85 kHz) [18]. Systems with large air gaps (10–40 cm) and low coupling factors (0.1–0.4) are modelled using admittance matrix approaches for steady-state current analysis in LCL topologies [9]. Beyond hardware, wireless V2G applications offer benefits such as peak load shaving and frequency regulation, while facing challenges like infrastructure limitations, battery degradation, and regulatory hurdles [19]. A medium-duty BWPT system integrating stationary energy storage, EVs, and a three-phase grid using SVPWM achieves near-unity power factor and reliable 20 kW operation [12]. These studies collectively emphasize the importance of coil design, resonant topology, control strategies, and standard compliance in advancing efficient and scalable BWPT systems for EV and grid integration.

III. BWPT DESIGN

At the resonance frequency, the power that is transferred from the initial coil to the secondary one can be expressed as,

$$\mathbf{P = \omega_0 M I_p I_S} \tag{1}$$

Where M represents the mutual-inductance that exists between the primary and secondary coils, I_p is the root-mean-square (rms) current of primary coil, I_S is the rms current in the secondary coil, and ω_0 is the resonance frequency. [21] A coupled inductor having a magnetising inductance between the coils can be expressed as,

$$\mathbf{L_M = k\sqrt{L_p L_S}} \tag{2}$$

Where L_p is the primary inductance, L_S is the secondary inductance, k is the coupling coefficient, and L_M is the magnetising inductance. The leakage inductances of the coil is expressed as,

$$\mathbf{L_{l,p} = L_p - L_M} \tag{3}$$

$$\mathbf{L_{l,s} = L_s - L_M} \tag{4}$$

Where $L_{l,p}$ is the leakage inductance of primary coil and $L_{l,s}$ is the leakage inductance of secondary coil. [7] For each turn the mutual inductance can be represented as,

$$\mathbf{\hat{M} = k\left(\hat{L}_P \hat{L}_S\right)^{1/2}} \tag{5}$$

The value of $\hat{M}$ is decided by the dimension of the charging pads and the air gap between them. [14] The voltage induced on the secondary coil is derived from the Faraday's law

$$\mathbf{v_S = M\frac{di_p}{dt}} \tag{6}$$

Where v_S is the induced voltage, M is the mutual inductance between the coils, i_p is the current through the primary coil. In case of "sinusoidal quantities" the equation (6) can be written according to Steinmetz transform as,

$$\mathbf{\bar{v_s} = j\omega_{HF} M \bar{I}_p} \tag{7}$$

Where $\bar{v_s}$ is the peak value of induced voltage v_S, $\bar{I}_p$ is the peak value of current through the primary coil i_p, ω_{HF} is the supply angular frequency, and M is the mutual inductance.

SAE J2954 Standard

SAE J2954 specifies wireless charging requirements for light-duty EVs, including four power classes (up to 22 kVA) and efficiency targets. It defines a nominal frequency of 85 kHz (79–90 kHz allowed) for the inductive link. The system efficiency as per equation 8 must meet a minimum level given by (8) under aligned conditions. The standard requires about 85% end-to-end efficiency. Assuming 92% coil coupling (based on [22]) implies that power electronics must achieve very high efficiency (see (9)). These criteria guide the BWPT design to meet industry benchmarks.

$$\mathbf{\eta_{tot} = \frac{p_B}{p_G} \geq 0.80} \tag{8}$$

Where $\frac{p_B}{p_G}$ is the ratio between the active power fed into the battery and the power discharged from the grid.

$$\mathbf{\eta_C = \frac{\eta_{tot}}{\eta_t} = \frac{0.85}{0.92} = 0.92} \tag{9}$$

The load resistance of the secondary side tuning network at its output can be expressed as,

$$\mathbf{R_{L,batt} = \frac{8}{\pi^2}\frac{V_{batt}^2}{P_{batt}}} \tag{10}$$

The comparable ac resistance at the input of resonant tank can be expressed as,

$$\mathbf{R_{L,dC-link} = \frac{8}{\pi^2}\frac{V_{dc\_link}^2}{P_{dc\_link}}} \tag{11}$$

n represents the primary to secondary coil turns ratio, which is given as,

$$\mathbf{n = \sqrt{\frac{L_s}{Lp}}} \tag{12}$$

If each system component satisfies the requirements for resonant frequency adjustment ω_0 as,

$$\mathbf{\omega_0 = \frac{1}{\sqrt{L_{11}c_{11}}}} \tag{13}$$

And

$$\mathbf{\omega_0 = \frac{1}{(L_p - L_{11})C_{12}} = \frac{1}{(L_s - L_{22})C_{21}}} \tag{14}$$

Then, when the bidirectional system is in charging mode, the associated voltage transfer functions can be stated as,

$$\mathbf{|M_{v,charge}| = \left|\frac{v_{batt}}{v_{dc\_link}}\right|} \tag{15}$$

$$\mathbf{= \frac{\omega^2 L_M C_{11}}{(1-(\omega/\omega_0)^2 + j\omega c_{22} R_{L,batt})(1/C_{21} + J\omega L_s) + j\omega L_{22} + R_{L,dc\_link}}} \tag{16}$$

While the bidirectional system during discharge mode, the voltage transfer function can be stated in [7] as,

$$\mathbf{|M_{v,discharge}| = \left|\frac{v_{dc\_link}}{v_{batt}}\right|} \tag{17}$$

$$\mathbf{= \frac{\omega^2 L_M C_{22}}{(1-(\omega/\omega_0)^2 + j\omega c_{11} R_{L,dc\_link})(1/C_{12} + J\omega L_p) + j\omega L_{11} + R_{L,batt}}} \tag{18}$$

Quality factor (Q factor) and bandwidth: Electric and magnetic fields are detected by the currents and charges kept in the RLC circuit. The Q factor of a circuit with resonance frequency ω_0 is expressed as,

$$\mathbf{Q = \omega_0 \frac{W}{P}} \tag{19}$$

$$\mathbf{Q = 2\pi \frac{stored\ electric\ and\ maagnetic\ energy}{energy\ dissipated\ during\ one\ periode}} \tag{20}$$

Where p is resistive losses of power, W is net energy stored in electric and magnetic field, and ω_0 is resonance frequency.

[23] In WPT systems, smaller energy losses are generally indicated by higher Q-factors, which results in increased efficiency. Therefore, considering Q factor is crucial. The mutual inductance is explained in equation (5) and the coupling coefficient k is expressed in [24] as,

$$\mathbf{K} = \frac{\mathbf{M}}{\sqrt{\mathbf{L_1} \cdot \mathbf{L_2}}} \tag{21}$$

Where M is mutual coupling between the coils, L_1 and L_2 are self-inductances. The coupling coefficient *k*, which denotes the degree of coupling between the coils, has a major impact on a WPT system's efficiency. The equivalent impedances at resonance frequency can be expressed in [24] as,

$$\mathbf{Z_1} = \mathbf{R_s} + \mathbf{R_{1ac}} \tag{22}$$

$$\mathbf{Z_2} = \mathbf{R_l} + \mathbf{R_{2ac}} \tag{23}$$

Where R_{1ac} and R_{2ac} are the series resistance of primary and secondary coil, R_s and R_l are the source and load resistance.

IV. Simulink Design for Unidirectional Power Transfer

Fig. 2 illustrates the unidirectional WPT model. The grid-side AC input is rectified by a diode bridge to DC, then converted by a PWM-controlled H-bridge inverter into high-frequency AC. This AC drives the LCC resonant network (loosely coupled inductors and capacitors) tuned to the operating frequency, maximizing transfer efficiency. On the vehicle side, the high-frequency AC is rectified back to DC and then processed by a DC–DC converter (with a freewheeling diode) to regulate the charging voltage. The freewheeling diode provides a current path when a switch is off. This setup demonstrates one-way G2V charging; enabling bidirectional flow would require replacing these stages with bidirectional converters and appropriate control logic.

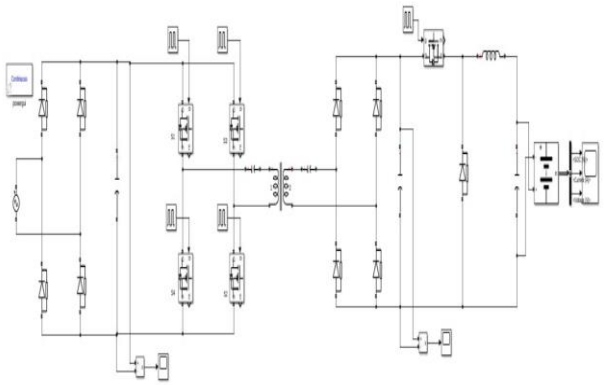

Figure 2: Simulink model of Unidirectional wireless power transfer system.

V. Simulink Design of BPWT System

Fig. 3 illustrates the **Simulink model of the primary side** (grid interface), which represents the first half of the proposed Bidirectional Wireless Power Transfer (BWPT) system. Correspondingly, Fig. 4 presents the **Simulink model of the secondary side** (vehicle interface), completing the BWPT system architecture. The proposed system enables **bidirectional energy transfer** between the electric grid and electric vehicles (EVs), supporting both **Grid-to-Vehicle (G2V)** and **Vehicle-to-Grid (V2G)** modes. In G2V mode, the grid delivers energy to charge the EV battery. Conversely, in V2G mode, the energy stored in the EV battery can be supplied back to the grid, contributing to **smart grid balancing, frequency regulation, and peak load shaving**.

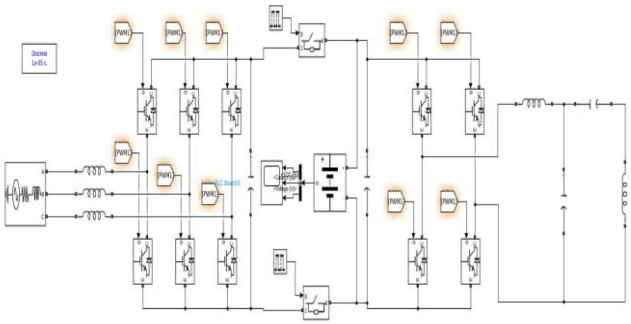

Figure 3: Simulink model of primary side of the BWPT system.

Additionally, a stationary **energy storage system** (battery) connected to the primary-side DC bus can supplement power delivery or absorb excess power, enhancing system flexibility and stability. **Bi-directional power control** is achieved by intelligent switching and modulation strategies. In G2V mode, energy flows from the grid to the EV. While in V2G mode, the roles of the power electronics are reversed: The **three-phase converter** on the grid side operates as a rectifier in G2V and as an inverter in V2G. The **H-bridge inverter** on the primary side functions as an inverter in G2V and as a rectifier in V2G. The **vehicle-side rectifier** becomes an inverter in V2G, sending energy from the EV back to the grid.

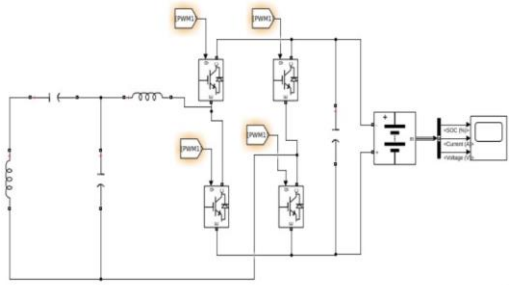

Figure 4: Simulink model of secondary side of the BWPT system.

Fig. 5 illustrates the circuit diagram of the resonant stage, detailing the configuration of the WPT coils and associated resonant components (LCC compensation). This resonant interface is central to maintain high efficiency across a wide range of power levels and operating frequencies, by resonant components (LCC compensation). By enabling bidirectional energy flow and incorporating grid-interactive functionalities, the proposed BWPT system supports the broader adoption of **smart, sustainable, and resilient energy infrastructure** for the future of electric mobility.

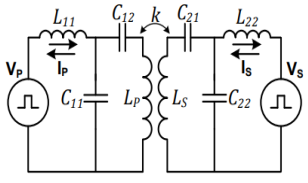

Figure 5: "LCC / LCC resonant stage of wireless power link." [7]

VI. METHODOLOGY

The BWPT system is modeled in MATLAB/Simulink using the parameters listed in Table 1. Key components include:

- **Grid-side AC Source:** Three-phase, 480 V nominal.
- **Grid-side Rectifier:** Six-switch (IGBT/diode) AC–DC converter.
- **DC-Link Capacitor:** Smooths and buffers the rectified voltage.
- **Bidirectional Switches:** Digital-controlled switches that select G2V or V2G mode.
- **H-Bridge Inverter:** Four-switch converter generating high-frequency AC for the wireless link.
- **Resonant Transformer (LCC Network):** Inductors and capacitors providing compensation for efficient coupling.
- **Vehicle-side Rectifier:** H-bridge converting received AC back to DC.
- **EV Battery:** 320–400 V pack storing energy (charging in G2V, discharging in V2G).
- **PWM Control:** Generates gate signals for all power-electronic switches.

For simulation purposes, the EV battery is modeled with an estimated capacity of 22 kWh and a nominal voltage of 400 V, representing typical mid-range electric vehicles. This assumption aligns with the observed SOC variations under a rated power transfer of 20 kW, enabling a practical evaluation of energy flow dynamics during G2V and V2G operation within realistic timeframes.

Table 1: System parameters [7]

Parameter	Value
Three-phase voltage source	480 V
Grid side battery	320 – 400 V
Nominal power (for both V2G and G2V)	20 kW
Dc link voltage	350 V
L11	52.1 µH
L22	37.6 µH
C11	1 µF
C12	0.67 µF
C22	1.33 µF
C21	0.57 µF
Lp	129.95 µH
Ls	125.4 µH
Vehicle side battery	320 – 400 V
Battery Capacity	22KWh
Resonance frequency	22 kHz

Table 1 provides all inductance, capacitance, voltage, and power values used in the model and Fig. 6 provides a flowchart of the proposed design.

Bidirectional Switches: Two ideal switches are included to control the direction of power flow. These switches will be governed by clock signals:

- **Clock signal "1"** enables the G2V mode by allowing current from the grid to the vehicle.
- **Clock signal "0"** disables G2V and enables V2G mode, isolating the grid input while allowing energy to flow from the vehicle to the grid.

A. Modes of Operation

Grid-to-Vehicle (G2V) Mode: In G2V mode, the grid supplies power to the EV. The grid-side rectifier and inverter converts AC to high-frequency AC for the transmitter coil, and the receiver coil at the vehicle side receives AC voltage which is rectified back to DC to charge the battery. In this mode, the grid converter functions as an inverter (supplying power) and the vehicle converter acts as a rectifier. Control signals enable current flow toward the EV battery and block reverse flow. **Clock logic:** The **rectifier receives clock signal "1"**, enabling current flow. The **inverter switches are disabled (clock signal "0")**, preventing reverse power flow.

Vehicle-to-Grid (V2G) Mode: In V2G mode, the EV battery becomes the power source. The vehicle-side inverter generates high-frequency AC sent through the resonant link, and the grid-side rectifier (now acting as a converter) captures this AC and returns DC to the grid or grid-side storage. The converter roles are swapped: the grid-side converter now rectifies incoming energy, and the vehicle-side converter acts as inverter. Switching signals ensure safe and efficient power transfer back to the grid. **Clock logic:** The **inverter receives clock signal "1"** to operate. The **rectifier is disabled (clock signal "0")**, preventing AC injection back into the vehicle-side DC bus.

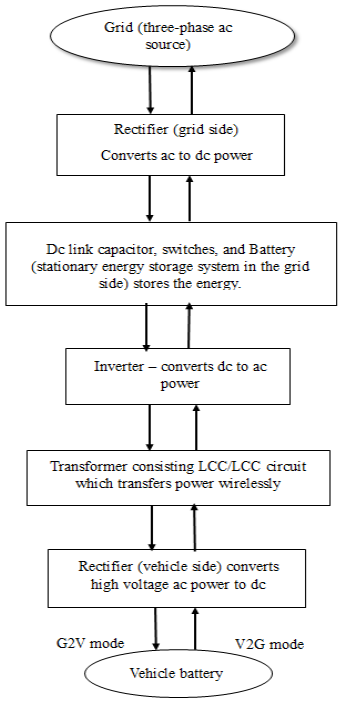

Figure 6: Flowchart of the proposed design.

VII. RESULTS AND DISCUSSION

This section presents the simulation results of the proposed **Bidirectional Wireless Power Transfer (BWPT)** system, designed to facilitate both **Grid-to-Vehicle (G2V)** and **Vehicle-to-Grid (V2G)** power flow. The simulation was carried out using **MATLAB/Simulink**, utilizing the key system parameters outlined in **Table 1**. The model captures the complete bidirectional operation, including the behaviour of power electronic converters, the resonant wireless link (LCC/LCC circuit), and the dynamic response of energy storage elements at both the grid and vehicle ends. All the graphs are simulated on a second time scale considering the

complexity of the simulation except for the BWPT V2G mode where the discharge to grid from vehicle happens at a faster rate for the chosen battery capacity.

A. Result of Unidirectional Wireless Power Transfer

Fig. 7 presents the simulation results of the **Unidirectional Wireless Power Transfer (WPT)** system, focusing on three critical performance metrics: **State of Charge (SOC)**, **Charging Current**, and **Battery Voltage**.

State of Charge (SOC): The SOC plot exhibits a steady upward trend for 10 sec, indicating continuous energy transfer from the grid to the vehicle.

Charging Current (A): The current profile initially displays high charging current that gradually decreases over time. This behavior aligns with standard battery charging protocols, where current tapers off as the battery approaches full capacity to prevent overcharging and ensure safety.

Battery Voltage (V): The voltage curve initially rises and then stabilizes or slightly declines. This plateau or minor drop is attributed to internal battery resistance and specific charging characteristics, potentially influenced by factors such as temperature, battery age, or chemistry.

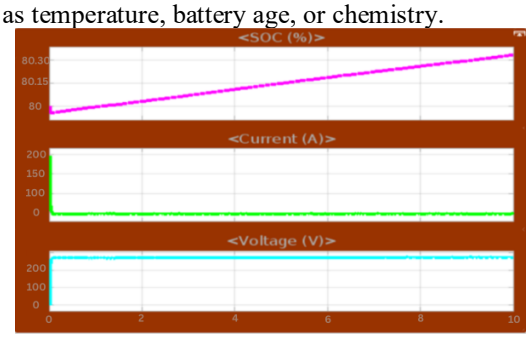

Figure 7: SoC, Current and Voltage Profile of UWPT with time(sec)in x-axis.

B. Results of BWPT on V2G

Once the battery reaches a lower SOC threshold, the voltage stabilizes, maintaining consistent energy delivery to the grid. These results verify the correct operation of the BWPT system under V2G mode, demonstrating its ability to reliably and efficiently return power to the grid while maintaining safe battery discharge conditions.

State of Charge (SOC%): Fig. 8 shows the SOC declining from 90% to 75%, confirming battery discharge during V2G operation.

Current (A): The green curve peaks at ~200 A and stabilizes around 0 A, reflecting the transition from steady-state discharge to cut-off at mentioned limit

Voltage (V): The grey trace drops from 350 V to ~286 V, consistent with typical lithium-ion battery discharge behaviour as SOC decreases.

C. Results of BWPT on G2V

Fig. 9 presents the simulation outcomes for the Bidirectional Wireless Power Transfer (BWPT) system during **Grid-to-Vehicle (G2V)** operation. This mode facilitates the energy flow from the grid to the electric vehicle (EV) battery, as evidenced by the increasing **State of Charge (SOC)** and supporting current and voltage behaviors. The plots validate the charging dynamics at the grid-side battery interface.

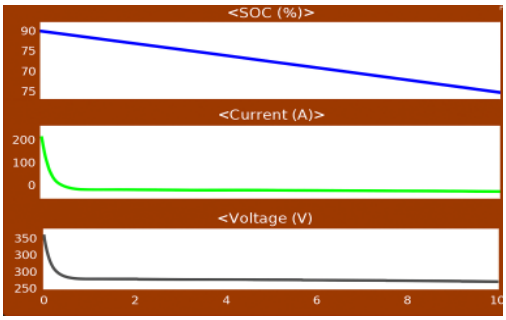

Figure 8: SoC, Current and Voltage Profile of BWPT on V2G with time(min)in x-axis.

State of Charge (SOC%): The SOC (blue trace) increases from 90.000% to ~90.015%, confirming G2V charging. The small rise reflects the short simulation window.

Current (A): The green curve holds steady at 200 A, and reduces to 0 as voltage takes control indicating consistent energy transfer and controlled charging behavior of Constant Current - Constant Voltage method

Voltage (V): The grey trace raises from ~310 V to 350 V, then stabilizes—typical of transient settling during battery charging.

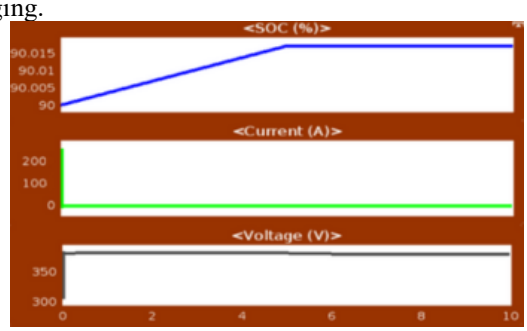

Figure 9: SoC, Current and Voltage Profile of BWPT on V2G with time(sec)in x-axis.

VIII. CONCLUSION

This research focuses on the design and simulation of a **Bidirectional Wireless Power Transfer (BWPT)** system, targeting enhanced efficiency and reliable bidirectional energy exchange between the power grid and electric vehicles (EVs). A robust control strategy was developed and implemented to enable **seamless transitions** between **Grid-to-Vehicle (G2V)** and **Vehicle-to-Grid (V2G)** operation modes. This approach presents a practical framework for integrating EVs as active components within modern smart grids. The system was tuned to operate at a **resonant frequency of 22 kHz**, with appropriately selected inductance and capacitance values to achieve efficient resonant inductive coupling. This enabled the WPT system to maintain high performance under various operating conditions. Simulation of the proposed system was conducted using **MATLAB/Simulink**, validating theoretical models and demonstrating its feasibility for real-world application.

The simulation outcomes confirmed the high efficiency of the system, achieving:

- **97.4% efficiency in G2V mode**, and
- **90.25% efficiency in V2G mode**.

Additionally, a **unidirectional WPT system** was also simulated to benchmark performance, further reinforcing the superiority of the bidirectional configuration. Overall, the

findings underscore the **technical viability and practical relevance** of bidirectional wireless power transfer systems for future smart mobility and energy infrastructures.

ACKNOWLEDGMENT

The authors would like to thank **FEV UK Ltd.** for their support and valuable insights throughout the development of this research. Their contributions were essential in guiding the design and simulation work presented in this study.

REFERENCES

[1] "The global electric vehicle market overview in 2024". [online]. Available: https://www.virta.global/global-electric-vehicle-market [Accessed Aug. 3, 2024]

[2] "Trends in electric car" Apr. 2024. [online]. Available: https://www.iea.org/reports/global-ev-outlook-2024. [Accessed Aug. 4, 2024]

[3] Y. Yang, Y. Benomar, M. El Baghdadi, O. Hegazy and J. Van Mierlo, "Design, modeling and control of a bidirectional wireless power transfer for light-duty vehicles: G2V and V2G systems," *2017 19th European Conference on Power Electronics and Applications (EPE'17 ECCE Europe)*, Warsaw, Poland, 2017, pp. P.1-P.12, doi: 10.23919/EPE17ECCEEurope.2017.8099387.

[4] D. Ahmad *et al*., "A Bidirectional Wireless Power Transfer for Electric Vehicle Charging in V2G System," *2019 International Conference on Electrical, Communication, and Computer Engineering (ICECCE)*, Swat, Pakistan, 2019, pp. 1-6, doi: 10.1109/ICECCE47252.2019.8940646.

[5] Venkatesan, M.; Rajamanickam, N.; Vishnuram, P.; Bajaj, M.; Blazek, V.; Prokop, L.; Misak, S. A Review of Compensation Topologies and Control Techniques of Bidirectional Wireless Power Transfer Systems for Electric Vehicle Applications. *Energies* **2022**, *15*, 7816. https://doi.org/10.3390/en15207816

[6] U. K. Madawala and D. J. Thrimawithana, "A Bidirectional Inductive Power Interface for Electric Vehicles in V2G Systems," in *IEEE Transactions on Industrial Electronics*, vol. 58, no. 10, pp. 4789-4796, Oct. 2011, doi: 10.1109/TIE.2011.2114312.

[7] O. C. Onar *et al*., "20-kW Bi-directional Wireless Power Transfer System with Energy Storage System Connectivity," *2020 IEEE Applied Power Electronics Conference and Exposition (APEC)*, New Orleans, LA, USA, 2020, pp. 3208-3214, doi: 10.1109/APEC39645.2020.9124047.

[8] A. A. S. Mohamed, A. Berzoy and O. Mohammed, "Power Flow Modeling of Wireless Power Transfer for EVs Charging and Discharging in V2G Applications," *2015 IEEE Vehicle Power and Propulsion Conference (VPPC)*, Montreal, QC, Canada, 2015, pp. 1-6, doi: 10.1109/VPPC.2015.7352995.

[9] A. A. S. Mohamed, F. G. N. de Almeida and O. Mohammed, "Harmonics-based steady-state mathematical model of bidirectional inductive wireless power transfer system in V2G applications," *2016 IEEE Transportation Electrification Conference and Expo (ITEC)*, Dearborn, MI, USA, 2016, pp. 1-6, doi: 10.1109/ITEC.2016.7520197.

[10] Bertoluzzo, M.; Giacomuzzi, S.; Kumar, A. Design of a Bidirectional Wireless Power Transfer System for Vehicle-to-Home Applications. *Vehicles* **2021**, *3*, 406-425. https://doi.org/10.3390/vehicles3030025

[11] "Modeling, Analysis, and Implementation of Series-Series Compensated Inductive Coupled Power Transfer (ICPT) System for an Electric Vehicle" in Journal of Electrical and computer engineering, DOI:10.1155/2020/9561523

[12] A. Aktas, E. Aydin, O. C. Onar, G. -J. Su, B. Ozpineci and L. M. Tolbert, "Medium-Duty Delivery Truck Integrated Bidirectional Wireless Power Transfer System with Grid and Stationary Energy Storage System Connectivity," in *IEEE Journal of Emerging and Selected Topics in Power Electronics*, doi: 10.1109/JESTPE.2024.3429509.

[13] J. A. P. Lopes, P. M. R. Almeida, and F. J. Soares, "Using vehicle-to-grid to maximize the integration of intermittent renewable energy resources in islanded electric grids," 2009 International Conference on Clean Electrical Power, ICCEP 2009, pp. 290–295, 2009.

[14] M. Mohammad *et al*., "Bidirectional LCC–LCC-Compensated 20-kW Wireless Power Transfer System for Medium-Duty Vehicle Charging," in *IEEE Transactions on Transportation Electrification*, vol. 7, no. 3, pp. 1205-1218, Sept. 2021, doi: 10.1109/TTE.2021.3049138.

[15] Y. Tang, Y. Chen, U. K. Madawala, D. J. Thrimawithana and H. Ma, "A New Controller for Bidirectional Wireless Power Transfer Systems," in IEEE Transactions on Power Electronics, vol. 33, no. 10, pp. 9076-9087, Oct. 2018, doi: 10.1109/TPEL.2017.2785365.

[16] B. SARRAZIN, A. DERBEY, P. ALBOUY, J. -P. FERRIEUX, G. MEUNIER and J. -L. SCHANEN, "Bidirectional Wireless Power Transfer System with Wireless Control for Electrical Vehicle," *2019 IEEE Applied Power Electronics Conference and Exposition (APEC)*, Anaheim, CA, USA, 2019, pp. 3137-3143, doi: 10.1109/APEC.2019.8721800.

[17] C. S. Wong, J. Liu, L. Cao and K. H. Loo, "A SWISS-Rectifier-Based Single-Stage Three-Phase Bidirectional AC–DC Inductive-Power-Transfer Converter for Vehicle-to-Grid Applications," in IEEE Transactions on Power Electronics, vol. 38, no. 3, pp. 4152-4166, March 2023, doi: 10.1109/TPEL.2022.3220327.

[18] E. N. Esfahani, I. Bhattacharya, W. Adepoju and A. Olatunji, "Modeling and Tuning of Parameters of a Bidirectional Wireless Power Transfer For interfacing EVs with the DC Smart Grids," *2022 IEEE Vehicle Power and Propulsion Conference (VPPC)*, Merced, CA, USA, 2022, pp. 1-6, doi: 10.1109/VPPC55846.2022.10003443.

[19] H. Ben Sassi, F. Errahimi, N. Essbai and C. Alaoui, "V2G and Wireless V2G concepts: State of the Art and Current Challenges," 2019 International Conference on Wireless Technologies, Embedded and Intelligent Systems (WITS), Fez, Morocco, 2019, pp. 1-5, doi: 10.1109/WITS.2019.8723851.

[20] K. Song, C. Zhu, K. -E. Koh, D. Kobayashi, T. Imura and Y. Hori, "Modeling and design of dynamic wireless power transfer system for EV applications," IECON 2015 - 41st Annual Conference of the IEEE Industrial Electronics Society, Yokohama, Japan, 2015, pp. 005229-005234, doi: 10.1109/IECON.2015.7392922.

[21] G. A. Covic and J. T. Boys, "Modern Trends in Inductive Power Transfer for Transportation Applications," in IEEE Journal of Emerging and Selected Topics in Power Electronics, vol. 1, no. 1, pp. 28-41, March 2013, doi: 10.1109/JESTPE.2013.2264473.

[22] Robert W. Erickson, Fundamentals of Power Electronics. 31 Jan. 2001, pp 120-150.

[23] D. Ahmad et al., "A Bidirectional Wireless Power Transfer for Electric Vehicle Charging in V2G System," 2019 International Conference on Electrical, Communication, and Computer Engineering (ICECCE), Jul. 2019, doi: https://doi.org/10.1109/icecce47252.2019.8940646.

[24] Mohamed A. Hassan, A.Elzawawi " Wireless Power Transfer through Inductive Coupling" [online]. Available: https://www.inase.org/library/2015/zakynthos/bypaper/CIRCUITS/CIRCUITS-18.pdf [Accessed: August 20, 2024].